

Deep and stable interferometric nulling of broadband light with implications for observing planets around nearby stars

Kent Wallace, Graham Hardy & Eugene Serabyn

Jet Propulsion Laboratory, California Institute of Technology, MS 171-113, 4800 Oak Grove Drive, Pasadena, California 91109, USA

The number of indirectly detected planetary systems around nearby stars has grown tremendously since their initial discovery five years ago¹. But the direct observation of light reflected from these systems remains a formidable task, because of the high contrast ratios between them and their parent stars, and because of the tiny angular separations. Theoretically², these difficulties can be overcome by using a dual-aperture stellar interferometer in which the starlight is cancelled, or 'nulled', by broadband destructive interference, leaving the planet's light visible. Although the basic requirement of equal and oppositely directed electric fields is easy to state, an experimental demonstration of deep broadband nulling has been lacking, owing to difficulties engendered by the needs for extreme symmetry and stability, and low dispersion in the optical system. Here we report the deep (10^{-4}) and stable nulling of broadband (18% bandwidth) thermal light. These results validate the physical principles underlying future planet-searching interferometers, and our laboratory instrument will serve as a prototype for the nulling instrument to be implemented on the Keck interferometer in 2001.

The brightness contrast ratio of over $10^9:1$ between the Sun and the Earth at optical wavelengths implies that optically imaging such planets around nearby stars (separation is $0.1''$ at a distance of 10 pc) is impossible with present single-dish telescopes. On the other hand, the contrast ratio between a star and its attendant planets can theoretically be reduced² both by shifting to infrared wavelengths, where planetary thermal emission peaks, and by employing destructive interference between two collecting telescopes to cancel on-axis starlight. The problem then is to design a system in which the starlight cancellation is deep and broadband, as well as stable in time. Since the original conception³, several seemingly feasible approaches to deep, achromatic nulling have been proposed, but experimental verification has been lacking. These nulling schemes are based, respectively, upon a relative field-flip in a rotational shearing interferometer⁴⁻⁷ (RSI), a relative field inversion upon passage through focus⁸ and a phase retardation scheme^{9,10} in which each wavelength is delayed by a wavelength-independent π radians. Until now, the second¹¹ and third¹² approaches have achieved stellar rejections of approximately 5%, levels consistent with limitations set by optical quality and atmospheric fluctuations. Because mid-infrared null depths (defined as the inverse of the rejection ratio) of order 10^{-6} will eventually be needed for space-based terrestrial planet searches, it thus remains important to demonstrate that all of the experimental obstacles, such as fine path-length control, intensity balancing, low dispersion, wavefront clean-up, and polarization differences can indeed be overcome. Therefore we began with a series of laboratory experiments to validate the optical principles of deep nulling before the construction of an astronomical instrument. Optical wavelengths were used for these initial experiments because of their applicability to the planned nulling experiment on board NASA's Space Interferometer Mission¹³ (SIM), a location which will provide the first demonstration of nulling interferometry in space.

Our experimental set-up¹⁴ is based on the RSI approach^{4,5},

modified by the addition of polarization-compensating mirrors⁶ and the use of spatial filtering⁷ to effect wavefront clean-up. Our fibre-coupled RSI has already demonstrated very deep nulling of laser light^{14,15} with nulls over five orders of magnitude deep. The goals of our current set of experiments were to demonstrate that this nulling capability can be extended to a broad radiation bandwidth (that is, that an achromatic null can be achieved) and that the null can be stably maintained using only the weak signal from a thermal light source. In fact, we intentionally used a very faint white light signal, with a photon flux comparable to that expected from nearby stars on SIM. We also elected to begin with single-polarization light in order to test the feasibility of the optical scheme without the added complication of dual polarization operation (which would provide only a factor-of-two greater signal).

The details of our optical layout and the initial results with narrow-band laser radiation have been described previously^{14,15}, but several properties of the RSI warrant a quick review. First, the fundamental operational principle of the rotational shearing interferometer, the geometric field flip, is wavelength-independent. Second, since the beamsplitter is used in double-pass, each input beam is modulated by the same beamsplitter reflection/transmission product, thus automatically maintaining intensity balance for all wavelengths. Third, the reflections in the nuller are phase-compensated over all wavelengths by means of an additional fold mirror in each arm of the nuller⁷. Fourth, by coupling the focused output beam to a single mode fibre, only the core of the output point-spread function is detected, thus largely eliminating the effect of wavefront irregularities¹⁶. All of these special properties of the fibre-coupled RSI make it a singularly attractive architecture for nulling because it significantly relaxes the requirements on the optical coatings and surface quality. In terms of the experimental obstacles listed earlier, the only additional elements to consider are nanometre-level pathlength stability (to attain 10^{-4} nulls in the optical), and the minimization of dispersion.

It is worth noting the modifications made to the experiment in going from our previously reported laser results to wide-band operation. Our white-light source for these experiments is a quartz-halogen lamp coupled to the RSI through a single mode (for $\lambda > 500$ nm) optical fibre which provides a diffraction-limited star-like source. To eliminate dispersive dielectrics in the RSI, we accomplished the desired bandpass filtering and polarization selection before launching our light into free space. For this, we inserted

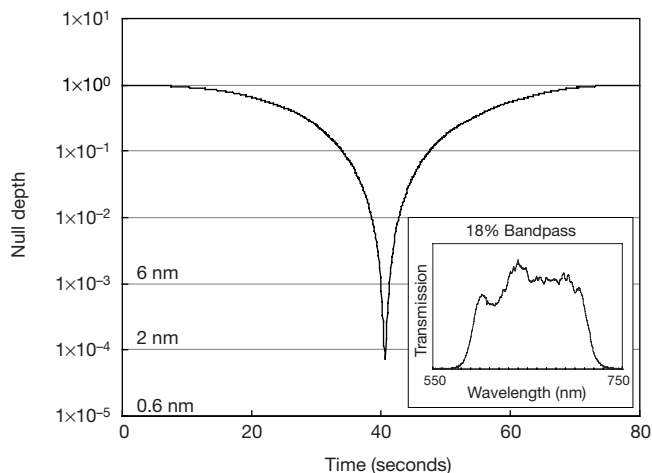


Figure 1 Intensity of the light transmitted through the nuller as the path length undergoes a linear sweep. The null depth is 7.4×10^{-5} in this scan. Each sample is 100 ms in duration. Inset, numbers on the y-axis represent the path-length match corresponding to the null depth scale; the chart is the spectral transmission of the light used in the measurements. The band-pass is roughly 590 nm to 710 nm, with a centre at 660 nm and a full-width at half-maximum of 120 nm, or 18%. The light is linearly polarized.

a miniature optical fibre bench with integral filters and polarizers between two fibres. We also added a fibre polarization-rotator to permit rotation of the single linear polarization state emerging from the fibre, thus allowing injection of white light with an arbitrary polarization orientation. We generally operate with s-plane polarization incident on the beamsplitter at 45°. The bandpass used in our experiment is roughly 'top hat' shaped, with a centre wavelength of 660 nm and a bandwidth of roughly 18% (Fig. 1). Our detector for the faint white light signal, a fibre-coupled avalanche photodiode (APD) was chosen to have sufficient dynamic range, without any gain change, to track the white light signal faithfully over at least five orders of magnitude (to see a 10⁻⁴ null unambiguously).

The location of the interferometer's zero optical path difference (OPD) fringe is found by translating one of the polarization compensation mirrors. A piezo-electric transducer (PZT) attached to a precision translation stage achieves a resolution of better than 1 nm. First, the deepest available destructive fringe is found by scanning in OPD through the white-light fringe packet. Dispersion in the system is determined by the asymmetry in the depth of the first destructive fringes to either side of the central fringe. Rotating the compensator to equalize the depths of these neighbouring fringes yields a local minimum in dispersion, and repeated optimization for successive fringes is used to find the global minimum null.

After precise alignment, a typical OPD scan through the null fringe is shown in Fig. 1. The null depth evident in this example is 7.1 × 10⁻⁵, thus verifying the ability of the fibre-coupled RSI to provide an achromatic null over this wide bandpass. In comparison, the deepest destructive fringe that a conventional Michelson interferometer could generate for a bandwidth of 18% is 7 × 10⁻³.

Path-length stabilization is the key to maintaining the null, and so to turning nulling into a useful technique for deep stellar rejection. Very small amplitude (~1 nm) path-length fluctuations between the two arms of the interferometer will degrade the null according to $N = (\varphi/2)^2$, where N is the null depth and φ is the phase error in radians. Because 1 nm is beyond the reach of typical metrology systems, the environment interior to the nuller must be made as stable as possible. To this end, the nuller is enclosed in Plexiglass and set upon a floating optical table with two levels of isolation (air legs and sorbothane pucks), the enclosure is lined with foam, and the optical mounts are all extremely rigid. Once the nuller is coarsely

aligned, fine alignment is done remotely from outside the sealed enclosure.

Even so, a path-length control scheme is needed to attain a stability level of the order of 1 nm. Several techniques have been proposed for this control, including use of a 'quadrature' output¹⁷ in an RSI, use of a waveband different for the nulling waveband¹², and of course, laser metrology. All of these techniques are under investigation, but for these initial experiments we opted for the much simpler approach of path-length dithering. This approach is standard in laser cavity stabilization, but as applied to nulling, the sign of the effect needs to be inverted to minimize the signal, and it must operate with far fewer photons. It might therefore be thought that the faint nulled signal is too weak to serve as an effective path-length error-sensing signal. However, since the error signal in dithering is given by the change in the photon flux relative to its value at the extremum, the error signals are exactly the same (except for sign) at a constructive peak and a destructive minimum. On the other hand, the photon noise is much reduced at null, resulting in an improvement in sensitivity (to OPD errors) that is proportional to the square root of the rejection ratio.

Figure 2 illustrates a dither-stabilized null in our fibre-coupled RSI. Under loop control, the null is stabilized to the 10⁻⁴ level (corresponding to a path-length stability of 2 nm), with an average null of approximately 7 × 10⁻⁵. The average photon detection rate at null was 145 photons per second. As our dither frequency is 20 Hz, the path-length control loop thus operates successfully with only 7 photons per dither cycle. Thus nanometer-level stabilization of a white-light null is evidently possible with a minuscule number of photons.

We note that our flux levels at null are quite comparable to those expected from nearby stars on both SIM and the proposed Terrestrial Planet Finder (TPF)¹⁸ mission. Assuming an aperture size for SIM of 30 cm, and a system transmission of 10%, the photon detection rate from a G2 star located 10 pc away in a 20% wide band centred at 0.7 μm is 1.1 × 10² photons per second when nulling to the 10⁻⁴ level. Thus the performance level achieved in our experiments (including the level of the null, its stabilization, and the photon rate at null) already meets the stringent requirements of the nulling experiment for SIM (except for dual-polarization operation). For TPF, operating in the mid-infrared with larger (~3 m)

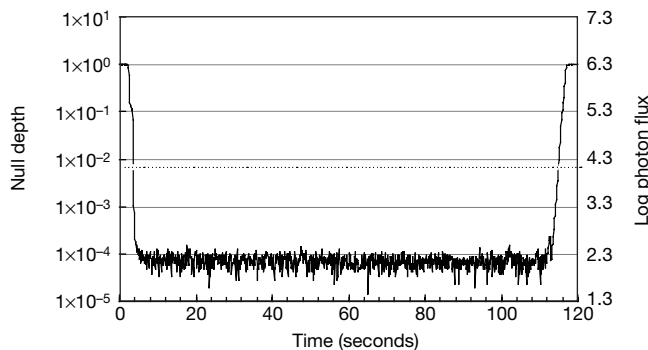


Figure 2 Illustration of the nuller output light under active control. The white-light signal begins high (at the first constructive fringe to one side of the null), is nulled (turned off) by changing the phase of the control loop by 180°, and then returned to its original level. Each sample is again 100 ms. Our analogue closed-loop dither scheme is implemented by applying a small-amplitude, sinusoidal voltage of frequency f to the piezo-electric transducer (PZT) that dithers the optical path difference (OPD) mirror with an amplitude of the order of 1 nm. The detected nuller optical output is then demodulated with a lock-in amplifier, which converts the component of the optical signal at frequency f to a d.c. error voltage. The OPD is driven to zero by adding this d.c. voltage to the dither signal applied to the PZT. The average null depth is about 7 × 10⁻⁵ under loop control with the worst null at about 1.4 × 10⁻⁴ and the best null of 1.4 × 10⁻⁵. The horizontal line represents the

deepest null level possible with chromatic, destructive interference in a standard Michelson interferometer. The right-hand side gives the corresponding photon fluxes. A 10⁻⁴ null corresponds to a detected flux of 200 photons per second. The reported null depths do not account for two effects that degrade our measured nulling performance: detector non-linearity at high fluxes, and dark counts (counts due to noise in the absence of any photons) at low fluxes. In the first case, with increasing photon flux, the detector increasingly sees overlapping, indistinguishable arrivals leading to an undercount at the constructive peak of about 20% for our conditions. The counts at null reported here also do not correct for the intrinsic noise floor of the detector, which artificially raises the count level at null (by about 30%). Both of these effects degrade the measured null depth from the true ratio, so that our true nulls are thus probably deeper by about 50%.

apertures, the residual photon flux at null may be about an order of magnitude smaller due to the deeper (10^{-6}) nulls required in this case, but more sensitive path length control schemes are under development^{12,17}. So with one option verified, and several more under test, the stabilization of the null need no longer be perceived as a large difficulty.

Although the viability of an optical nulling experiment at the 10^{-4} null level as planned for SIM is thus established, a final question is how this work may extrapolate to other experiments. In the near term, the RSI approach will be applied in a mid-infrared nulling instrument for use with the Keck Interferometer on Mauna Kea¹⁹ in 2001. As we begin to move our experiment from visible to infrared wavelengths, we anticipate our task of achieving deep nulls will be made easier, owing to the improved optical wave front quality and the reduced effect of path length fluctuations at long wavelengths (nanometre-level path length control is sufficient for a 10^{-6} mid-infrared null if path length fluctuations dominate), but also made more difficult by the lack of components such as single mode fibres for the mid-infrared, and the need to operate cryogenically. However, except for dual-polarization operation, the technical uncertainties in the RSI approach have largely been removed.

The American and European space communities are considering planet finders based on infrared nulling interferometry for early in the next decade^{18,20}. The final architecture for such missions is far from decided, as is the nulling approach to be used. At this point, each of the proposed nulling techniques seems to have its own specific advantages and disadvantages. For example, the beamsplitter needs to be exactly 50/50 in the phase retardation approach, whereas this stringent requirement is absent in RSIs. On the other hand, RSIs yield two nulled outputs instead of one, and so are somewhat more complicated. Thus, although further development is certainly necessary to achieve the requisite broadband, dual-polarization, 10^{-6} nulls in the mid-infrared, our experiments do provide validation for most of the physical principles upon which the final nuller must be based: an achromatic phase-shift of π radians between the electric fields, broadband operation, active path-length control, dispersion minimization, and wavefront clean-up by spatial filtering. □

Received 24 March; accepted 28 June 2000.

1. Mayor, M. & Queloz, D. A Jupiter-mass companion to a solar-type star. *Nature* **378**, 355–359 (1995).
2. Bracewell, R. N. Detecting nonsolar planets by spinning infrared interferometer. *Nature* **274**, 780–781 (1978).
3. Bracewell, R. N. & Macphie, R. H. Searching for nonsolar planets. *Icarus* **38**, 136–147 (1979).
4. Diner, D. J. in *The Next Generation Space Telescope* (eds Bely, P. Y., Burrows, C. J. & Illingworth, G. D.) 133–141 (Space Telescope Science Institute, Baltimore, 1990).
5. Shao, M. in *The Next Generation Space Telescope* (eds Bely, P. Y., Burrows, C. J. & Illingworth, G. D.) 160–168 (Space Telescope Science Institute, Baltimore, 1990).
6. Diner, D. J., Tubbs, E. F., Gaiser, S. L. & Korechhoff, R. P. Infrared imaging of extrasolar planets. *J. Br. Interplanet. Soc.* **44**, 505–512 (1991).
7. Shao, M. in *Space Astronomical Telescopes and Instrumentation* (eds Bely, P. Y. & Breckinridge, J. B.) *Proc. SPIE* **1494**, 347–356 (1991).
8. Gay, J. & Rabbia, Y. Principe d'un coronographe interférentiel. *C.R. Acad. Sci. Paris* **322**, 265–271 (1996).
9. Angel, J. R. P. in *The Next Generation Space Telescope* (eds Bely, P. Y., Burrows, C. J. & Illingworth, G. D.) 81–94 (Space Telescope Science Institute, Baltimore, 1990).
10. Angel, J. R. P., Burge, J. H. & Woolf, N. J. Detection and spectroscopy of exo-planets like Earth. *Proc. SPIE* **2871**, 516–519 (1996).
11. Badouze, P. et al. First results with the achromatic interfero coronagraph. *Proc. SPIE* **3353**, 455–462 (1998).
12. Hinz, P. M. et al. Imaging circumstellar environments with a nulling interferometer. *Nature* **395**, 251–253 (1998).
13. Danner, R. & Unwin, S. (eds) *Space Interferometry Mission (SIM)* 103–124 (JPL Brochure 400–811, Jet Propulsion Laboratory, Pasadena, 1999).
14. Serabyn, E., Wallace, J. K., Hardy, G. J., Schmidlin, E. G. H. & Nguyen, H. Deep nulling of visible laser light. *Appl. Opt.* **38**, 7128–7132 (1999).
15. Serabyn, E., Wallace, J. K., Nguyen, H. T., Schmidlin, E. G. H. & Hardy, G. J. in *Working on the Fringe: Optical and IR Interferometry from Ground and Space* (eds Unwin, S. & Stachnik, R.) 437–442 (ASP Conf. Ser. 194, Astronomical Society of the Pacific, San Francisco, 1990).
16. Ollivier, M. & Mariotti, J.-M. Improvement in the rejection rate of a nulling interferometer by spatial filtering. *Appl. Opt.* **36**, 5340–5346 (1997).
17. Serabyn, E. Nanometre-level path-length control scheme for nulling interferometry. *Appl. Opt.* **38**, 4213–4216 (1999).
18. Beichman, J. A., Woolf, N. J. & Lindensmith, C. A. (eds) *Terrestrial Planet Finder (TPF)* (JPL Publication 99-3, Jet Propulsion Laboratory, Pasadena, 1999).

19. Colavita, M. M. et al. The Keck Interferometer. *Proc. SPIE* **3350**, 776–784 (1998).

20. Leger, A. et al. Could we search for primitive life on extrasolar planets in the near future? The DARWIN project. *Icarus* **123**, 249–255 (1996).

Acknowledgements

We thank the Keck Interferometer and SIM projects for their support of this work. We also thank H. Nguyen for help with data acquisition. The work reported here was performed at the Jet Propulsion Laboratory, California Institute of Technology, under a contract with the National Aeronautics and Space Administration.

Correspondence and requests for materials should be addressed to K.W. (e-mail: James.K.Wallace@jpl.nasa.gov).

Superconductivity in molecular crystals induced by charge injection

J. H. Schön, Ch. Kloc & B. Batlogg

Bell Laboratories, Lucent Technologies, 600 Mountain Avenue, Murray Hill, New Jersey 07974-0636, USA

Progress in the field of superconductivity is often linked to the discovery of new classes of materials, with the layered copper oxides¹ being a particularly impressive example. The superconductors known today include a wide spectrum of materials, ranging in complexity from simple elemental metals, to alloys and binary compounds of metals, to multi-component compounds of metals and chalcogens or metalloids, doped fullerenes and organic charge-transfer salts. Here we present a new class of superconductors: insulating organic molecular crystals that are made metallic through charge injection. The first examples are pentacene, tetracene and anthracene, the last having the highest transition temperature, at 4 K. We anticipate that many other organic molecular crystals can also be made superconducting by this method, which will lead to surprising findings in the vast composition space of molecular crystals.

The experimental approach we followed is to inject a high concentration of charge carriers into organic molecular crystals of high quality, using a field-effect-transistor geometry (Fig. 1). There is a continuing effort to utilize a transverse static electric field in such an arrangement to modulate the properties of known superconductors². For example, the transition temperatures of copper oxide high-temperature superconductors can be varied significantly^{3–5}; this variation can be explained in terms of the known phase diagram of copper oxides, where the transition temperature changes systematically with the carrier concentration. More recently, the complete switching between an insulating and superconducting state has been reported in a fullerene field-effect transistor (FET)⁶. Our studies on organic molecular semiconductors, such as pentacene, revealed that low defect densities can be achieved in FET devices and that, in addition, the Fermi energy can be shifted through the bandgap leading to ambipolar transport⁷. Hence, the sign and concentration of charge carriers can be varied over an extremely wide range. The electronic structure of the

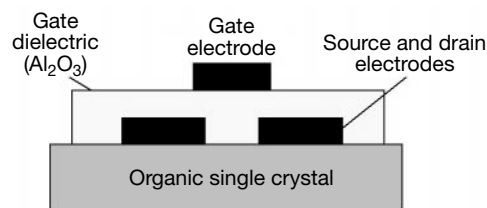


Figure 1 Schematic structure of an organic single crystal field-effect transistor.